University of Rijeka
Rijeka, Croatia

Detection of GW Signals Using Quadratic Time-Frequency Distributions and Deep CNNs

CA17137 g2net WG1 meeting

Valencia, 11 April 2022

Nikola Lopac, PhD

Time-Frequency Signal Representation

Non-Stationary Signals

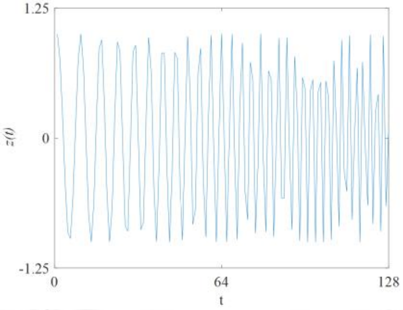

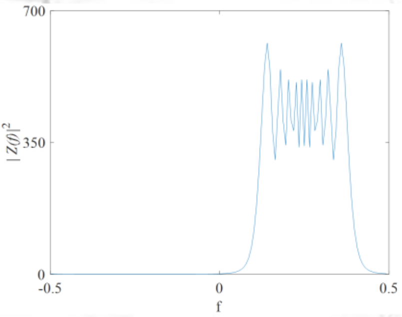

Non-stationary signals

- Time-varying frequency spectrum
- Multi-component
- Non-linear frequency modulation
- Noise

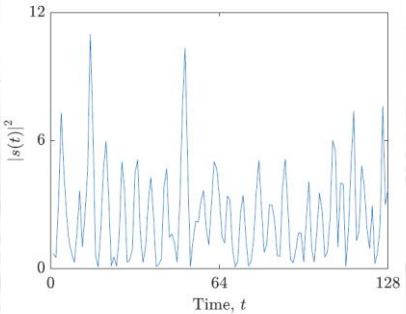

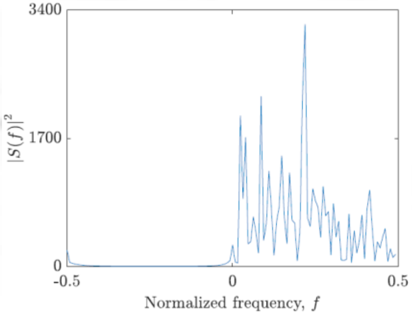

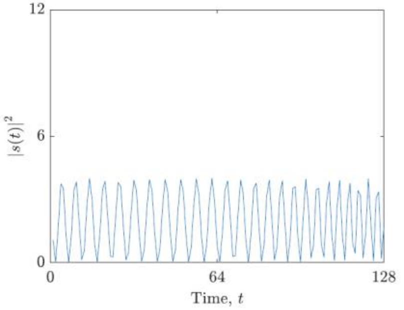

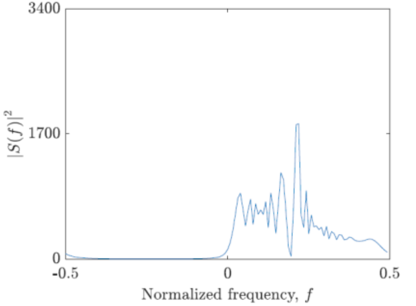

Time-Frequency Signal Representation

Signal representation in the joint time-frequency domain:

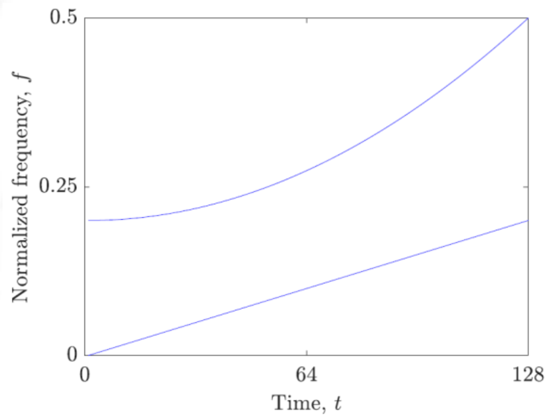

Linear time-frequency distributions

01

Signal decomposition into the elementary components well localized in time and frequency (STFT)

Quadratic time-frequency distributions

02

Time-frequency distributions (TFDs) (Cohen's class)

Spectrogram

Short-time Fourier transform (STFT):

$$STFT_s(t,f) = \int_{-\infty}^{\infty} s(\tau)h(\tau - t)e^{-j2\pi f\tau}d\tau$$

Spectrogram (SP):

$$SP_s(t,f) = \left|\int_{-\infty}^{\infty} s(\tau)h(\tau - t)e^{-j2\pi f\tau}d\tau\right|^2$$

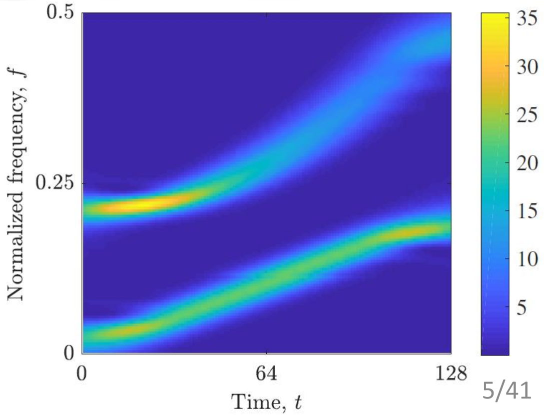

Cohen's Class TFDs

Wigner-Ville distribution (WVD):

$$WVD_s(t,f) = \int_{-\infty}^{\infty} s\left(t+\frac{\tau}{2}\right) s^*\left(t-\frac{\tau}{2}\right) e^{-j2\pi f\tau} d\tau$$

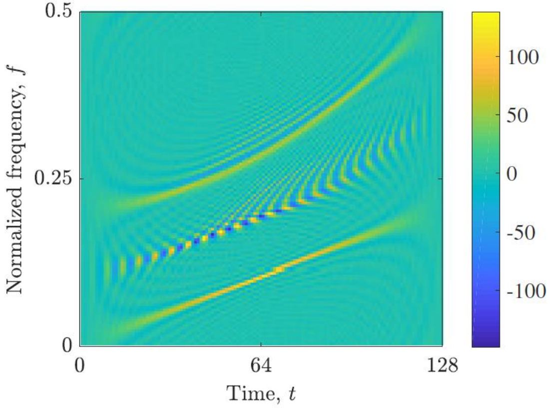

Pseudo Wigner-Ville distribution (PWVD):

$$PWVD_s(t,f) = \int_{-\infty}^{\infty} h(\tau)\, s\left(t+\frac{\tau}{2}\right) s^*\left(t-\frac{\tau}{2}\right) e^{-j2\pi f\tau} d\tau$$

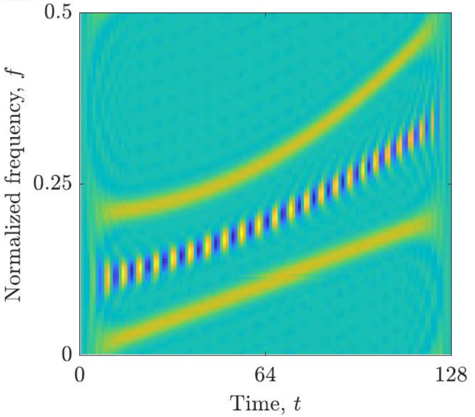

Cohen's Class TFDs

Smoothed pseudo Wigner-Ville distribution (SPWVD):

$$SPWVD_s(t,f) = \int_{-\infty}^{\infty} h(\tau) \int_{-\infty}^{\infty} g(u-t)\, s\left(u+\frac{\tau}{2}\right) s^*\left(u-\frac{\tau}{2}\right) du\, e^{-j2\pi f\tau} d\tau$$

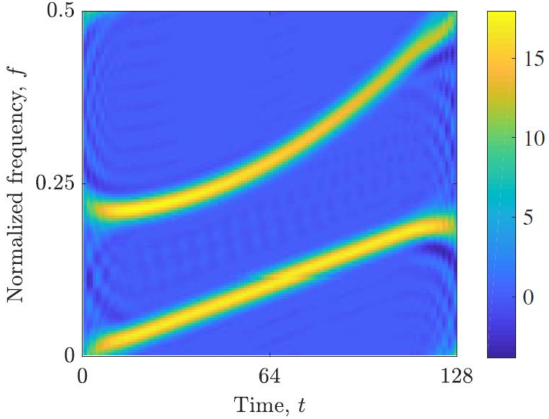

Choi-Williams distribution (CWD):

$$CWD_s(t,f) = \int_{-\infty}^{\infty} \int_{-\infty}^{\infty} \frac{\sqrt{\sigma}}{2\sqrt{\pi}|\tau|} e^{-\frac{u^2\sigma}{16\tau^2}} s\left(t+u+\frac{\tau}{2}\right) s^*\left(t+u-\frac{\tau}{2}\right) du\, e^{-j2\pi f\tau} d\tau$$

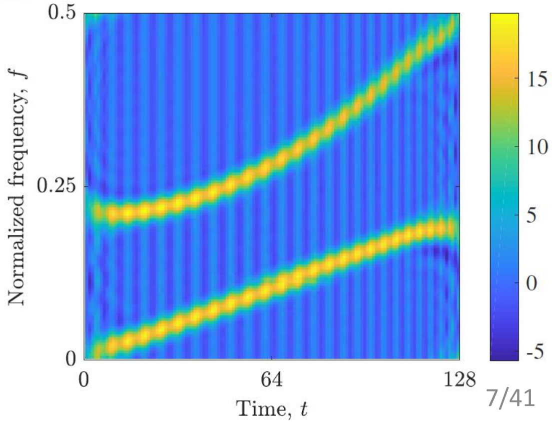

Cohen’s Class TFDs

Butterworth distribution (BUD):

$$BUD_s(t,f) = \int_{-\infty}^{\infty}\int_{-\infty}^{\infty} \frac{\sqrt{\sigma}}{2|\tau|} e^{-\frac{|u|\sqrt{\sigma}}{|\tau|}} s\left(t+u+\frac{\tau}{2}\right) s^*\left(t+u-\frac{\tau}{2}\right) du\, e^{-j2\pi f\tau} d\tau$$

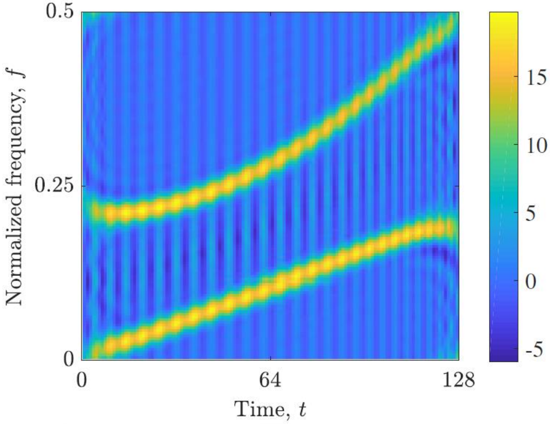

Born-Jordan distribution (BJD):

$$BJD_s(t,f) = \int_{-\infty}^{\infty} \frac{1}{|\tau|} \int_{t-\frac{|\tau|}{2}}^{t+\frac{|\tau|}{2}} s\left(u+\frac{\tau}{2}\right) s^*\left(u-\frac{\tau}{2}\right) du\, e^{-j2\pi f\tau} d\tau$$

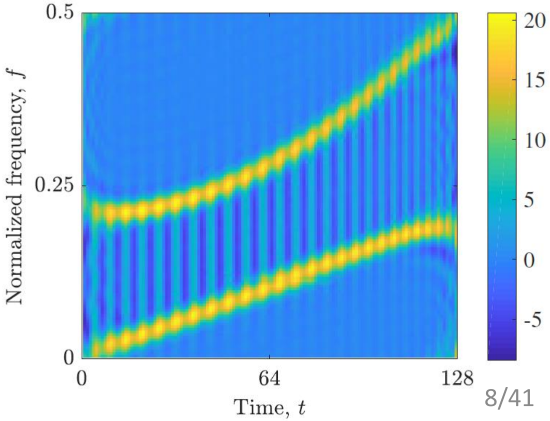

Cohen's Class TFDs

Zhao-Atlas-Marks distribution (ZAMD):

$$ZAMD_s(t,f) = \int_{-\infty}^{\infty} h(\tau) \int_{t-\frac{|\tau|}{2}}^{t+\frac{|\tau|}{2}} s\left(u+\frac{\tau}{2}\right) s^*\left(u-\frac{\tau}{2}\right) du\, e^{-j2\pi f\tau} d\tau$$

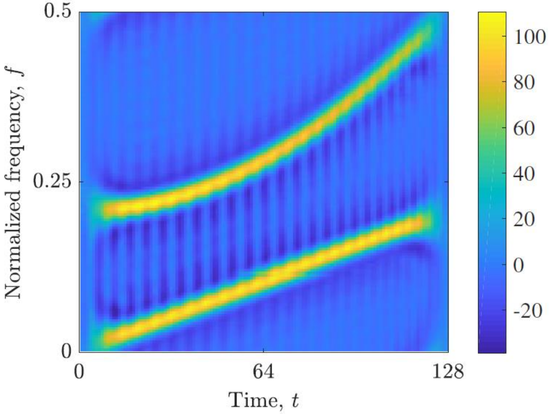

Reduced-interference distribution with a kernel based on the Bessel function (RIDB):

$$RIDB_s(t,f) =$$

$$\int_{-\infty}^{\infty} h(\tau) \int_{t-|\tau|}^{t+|\tau|} \frac{2g(u)}{\pi|\tau|} \sqrt{1-\left(\frac{u-t}{\tau}\right)^2}\, s\left(u+\frac{\tau}{2}\right) s^*\left(u-\frac{\tau}{2}\right) du\, e^{-j2\pi f\tau} d\tau$$

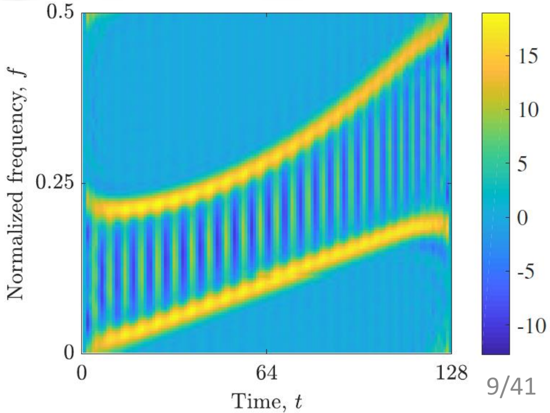

Cohen's Class TFDs

Reduced-interference distribution with a kernel based on the binomial coefficients (RIDBN):

$$RIDBN_s(t,f) = \sum_{\tau=-\infty}^{\infty} \sum_{u=-|\tau|}^{|\tau|} \frac{1}{2^{2|\tau|+1}} \binom{2|\tau|+1}{|\tau|+u+1} s[t+u+\tau]\, s^*[t+u-\tau]\, e^{-j4\pi f\tau}$$

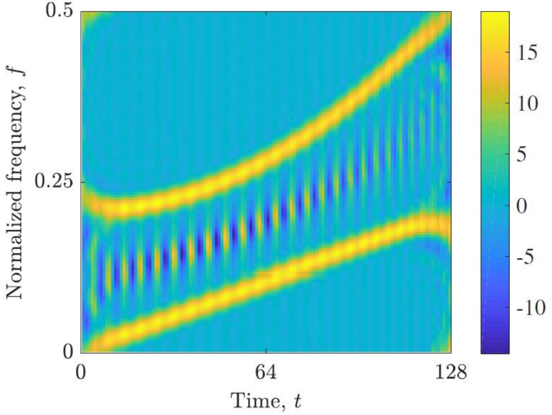

Reduced-interference distribution with a kernel based on the Hanning window (RIDH):

$$RIDH_s(t,f) = \int_{-\infty}^{\infty} h(\tau) \int_{-\frac{|\tau|}{2}}^{\frac{|\tau|}{2}} \frac{g(u)}{|\tau|} \left(1 + cos\left(\frac{2\pi u}{\tau}\right)\right) s\left(t+u+\frac{\tau}{2}\right) s^*\left(t+u-\frac{\tau}{2}\right) du\, e^{-j2\pi f\tau} d\tau$$

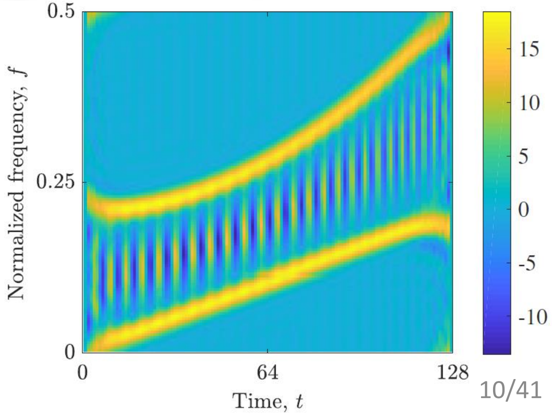

Cohen's Class TFDs

Reduced-interference distribution with a kernel based on the triangular window (RIDT):

$$RIDT_s(t,f) =$$
$$\int_{-\infty}^{\infty} h(\tau) \int_{-\frac{|\tau|}{2}}^{\frac{|\tau|}{2}} \frac{2g(u)}{|\tau|}\left(1-\frac{2|u|}{|\tau|}\right) s\left(t+u+\frac{\tau}{2}\right) s^*\left(t+u-\frac{\tau}{2}\right) du\, e^{-j2\pi f\tau} d\tau$$

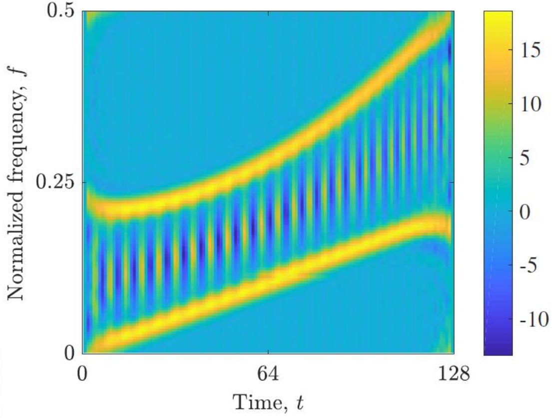

Deep Learning

Convolutional Neural Networks (CNNs)

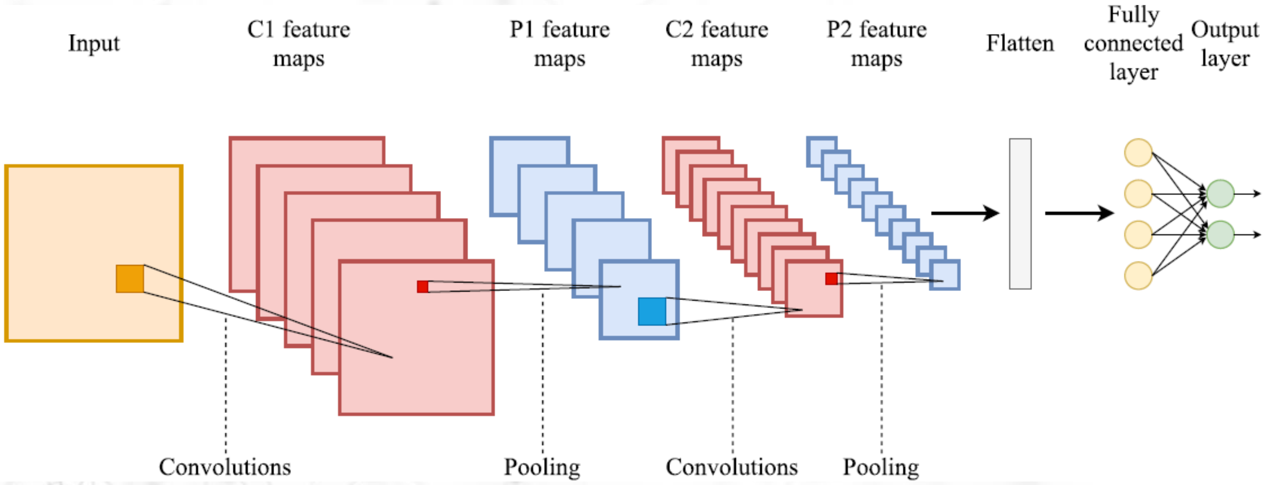

Research Objectives and Hypotheses

Research Objectives and Hypotheses

Method for detecting BBH GW signals in intensive noise
(TFDs from Cohen's class + deep learning)

High-performance detection of BBH GW signals in intensive noise

Better-structured information → higher classification performances than utilizing only the original noisy time-series signals

Proposed Method for Detecting GW Signals

Detection Procedure

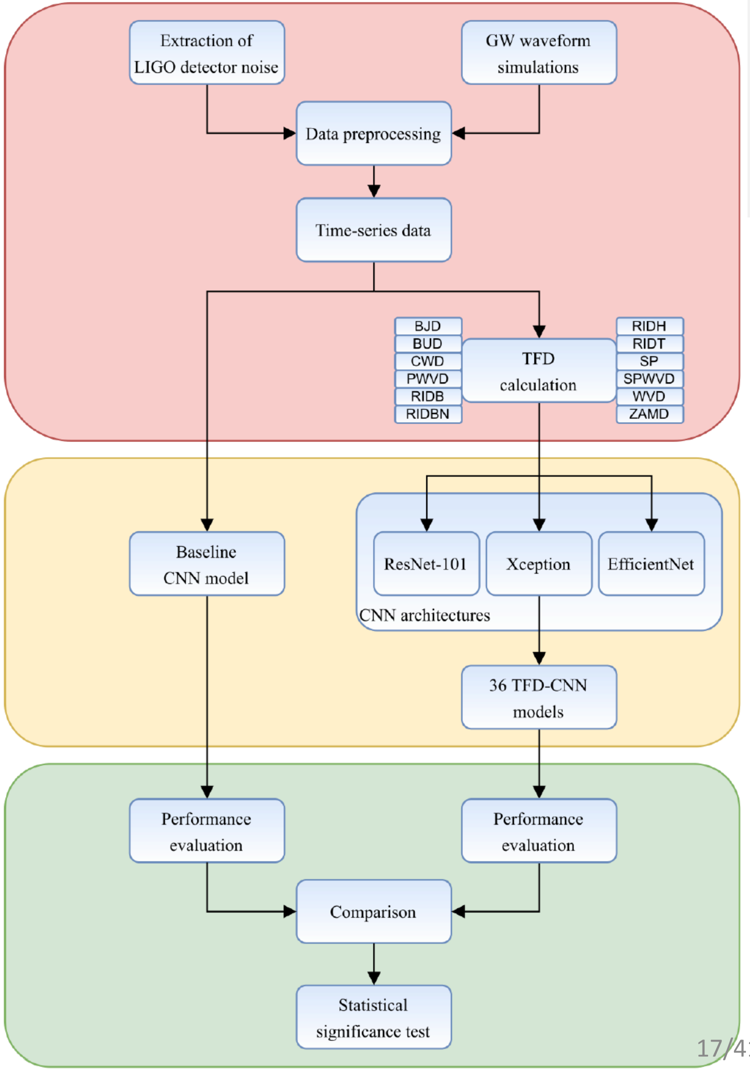

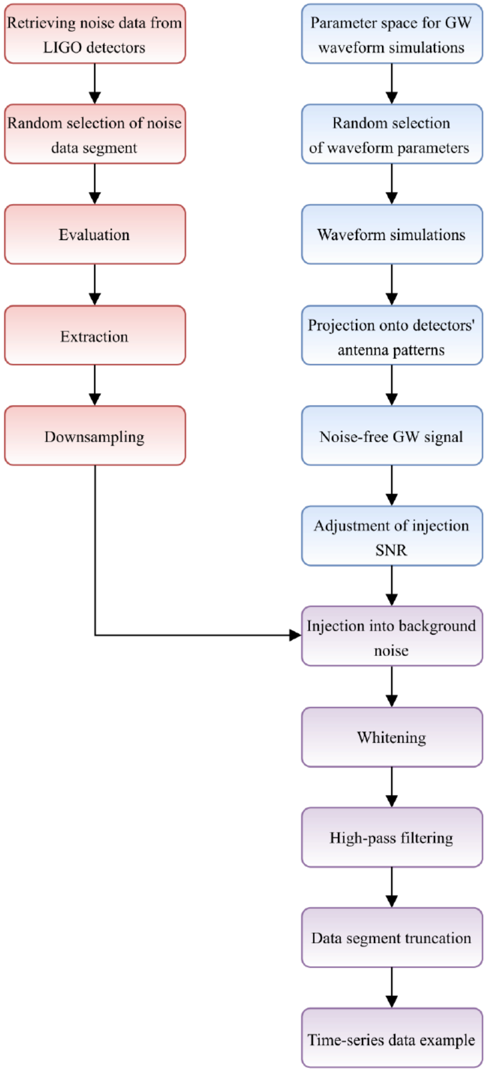

Data Generation

- Collecting LIGO detector recordings
- Simulations of GW waveforms
- Data preprocessing
- Time-series data

Time-Series Data

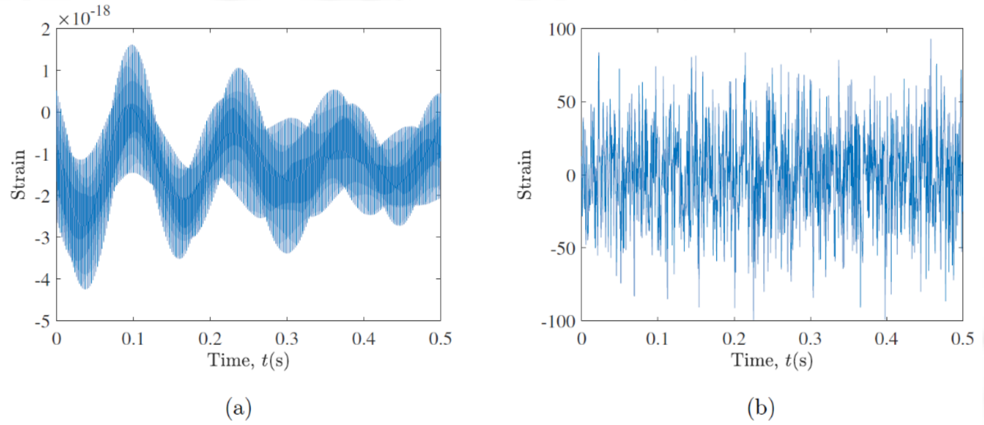

Noise

Time-Series Data

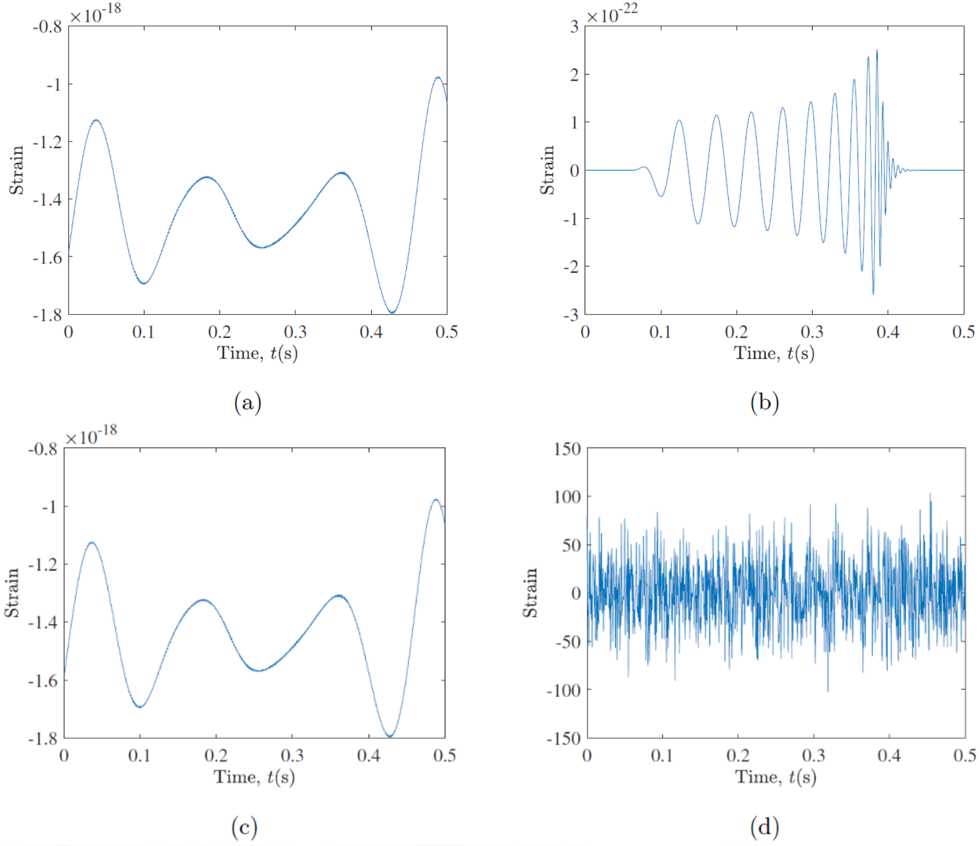

Data example containing GW signal in the noise (NOMF-SNR = 8 dB, OMF-SNR = 6.55 dB)

Time-Series Data

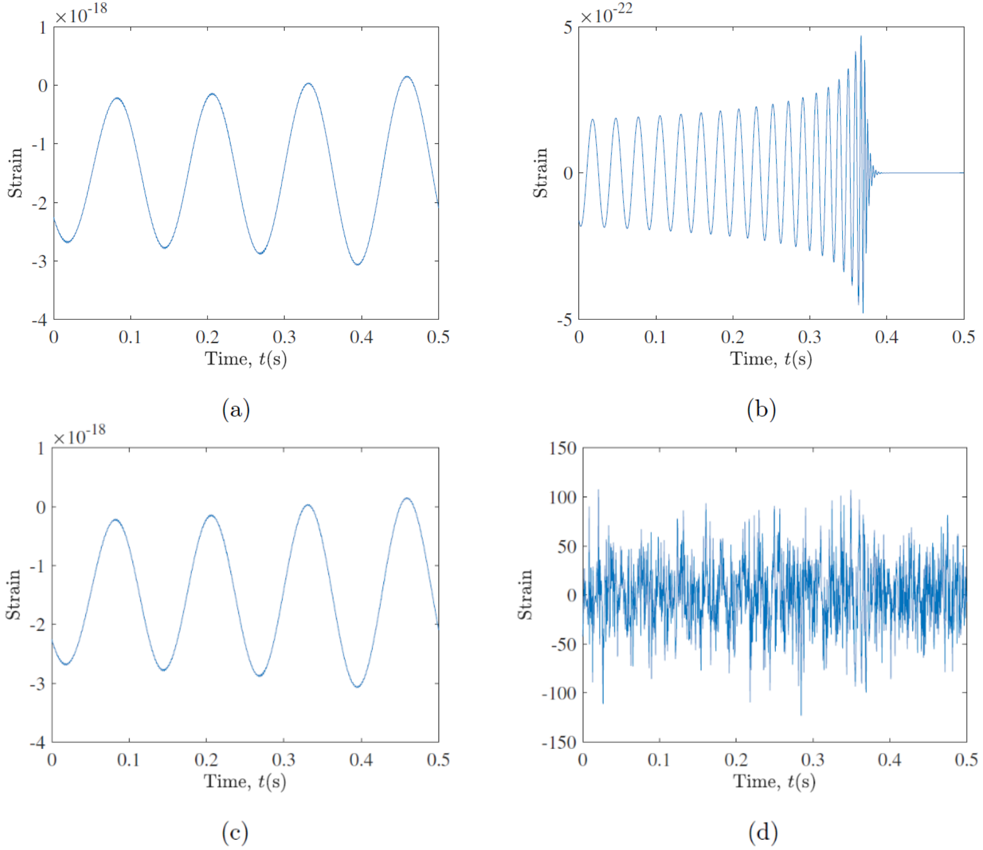

Data example containing GW signal in the noise (NOMF-SNR = 19 dB, OMF-SNR = 14.92 dB)

Time-Series Data

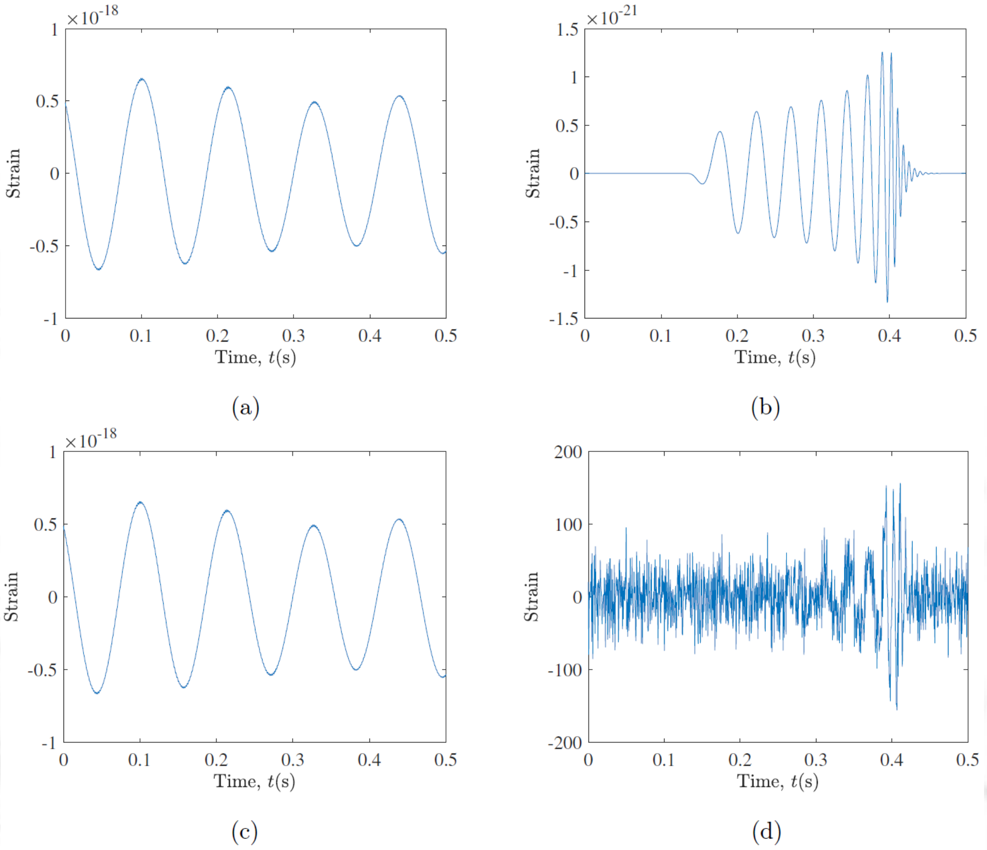

Data example containing GW signal in the noise (NOMF-SNR = 30 dB, OMF-SNR = 25.82 dB)

TFD Calculation

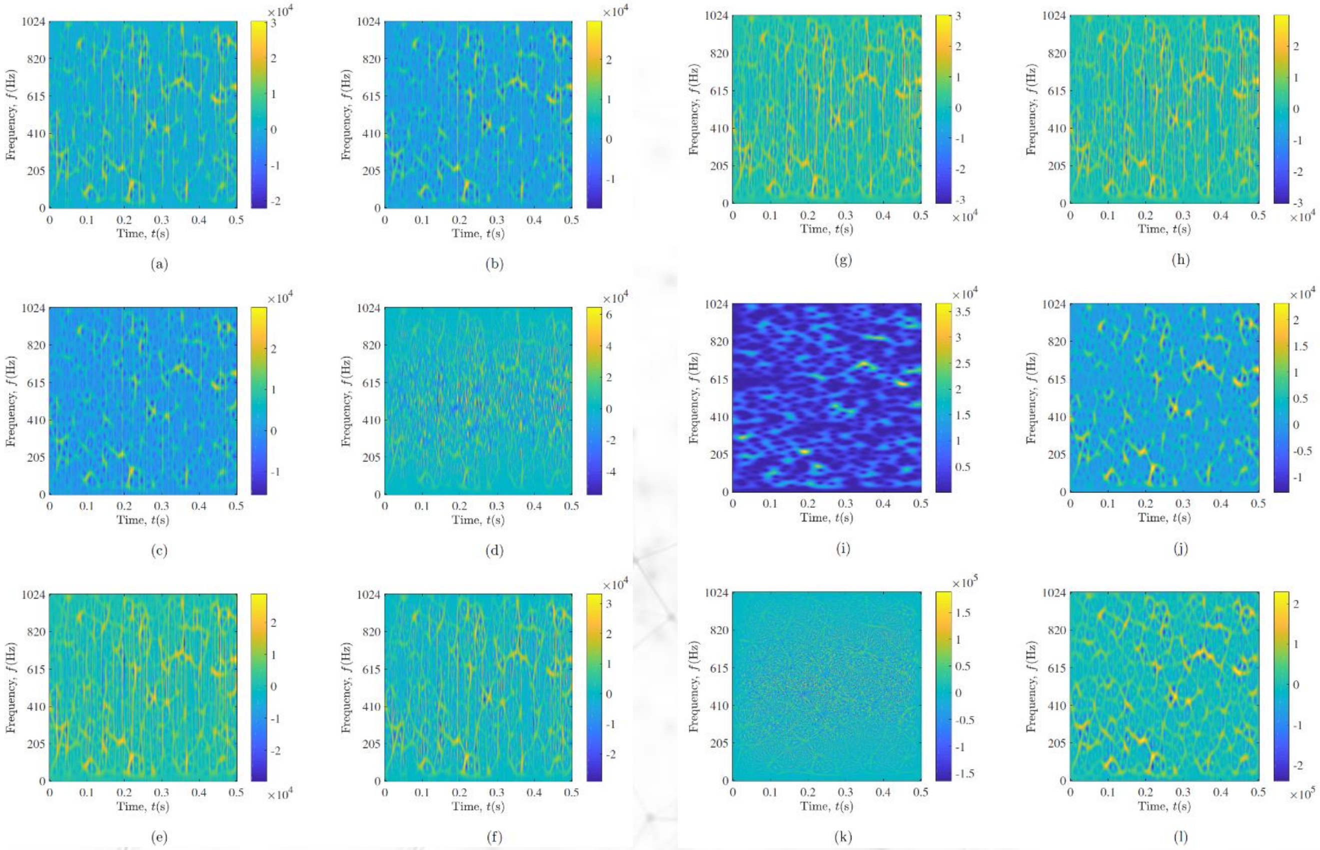

TFDs of the time-series data example containing only noise: (a) BJD; (b) BUD; (c) CWD; (d) PWVD; (e) RIDB; (f) RIDBN; (g) RIDH; (h) RIDT; (i) SP; (j) SPWVD; (k) WVD; (l) ZAMD.

TFD Calculation

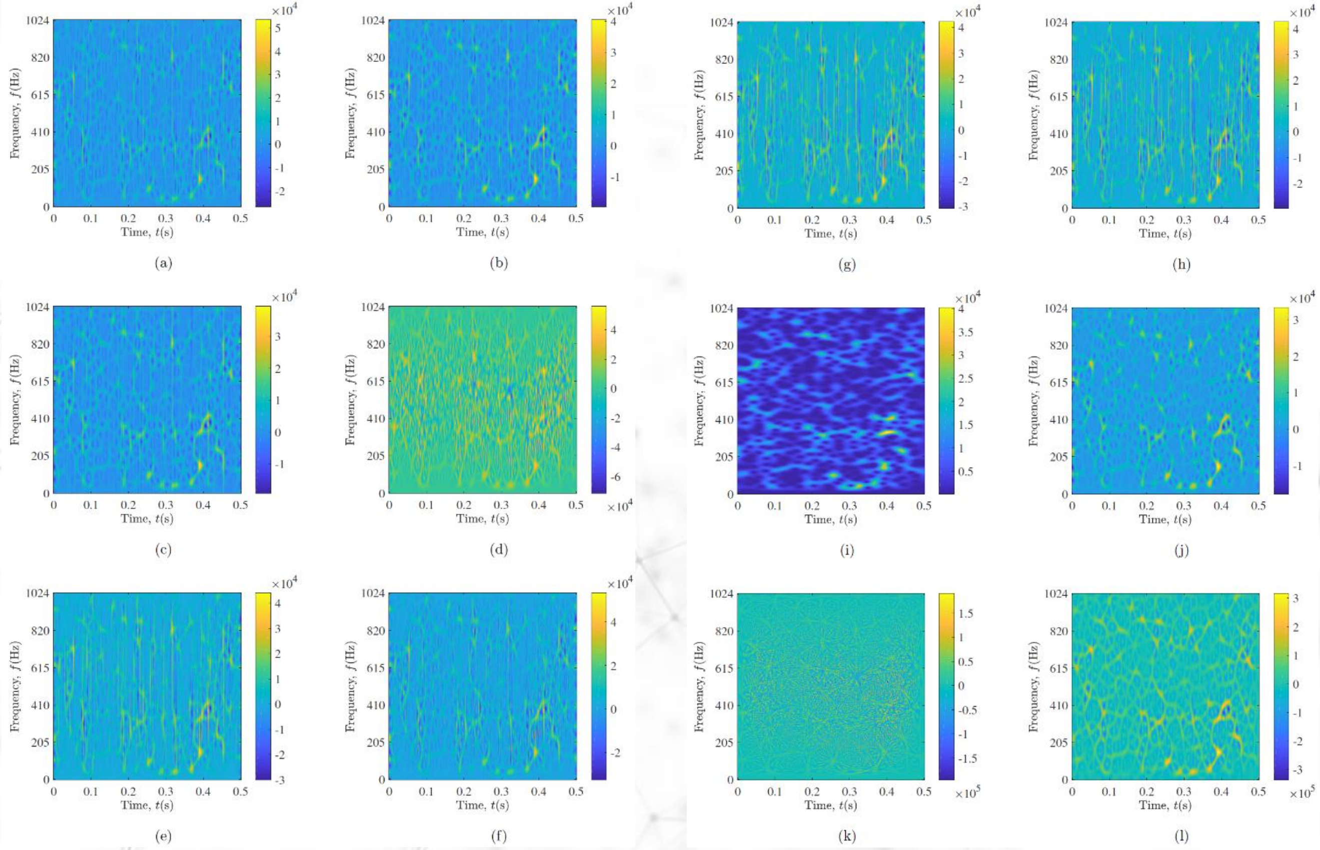

TFDs of the time-series data example containing the GW signal in the noise (NOMF-SNR = 8 dB, OMF-SNR = 6.55 dB): (a) BJD; (b) BUD; (c) CWD; (d) PWVD; (e) RIDB; (f) RIDBN; (g) RIDH; (h) RIDT; (i) SP; (j) SPWVD; (k) WVD; (l) ZAMD.

TFD Calculation

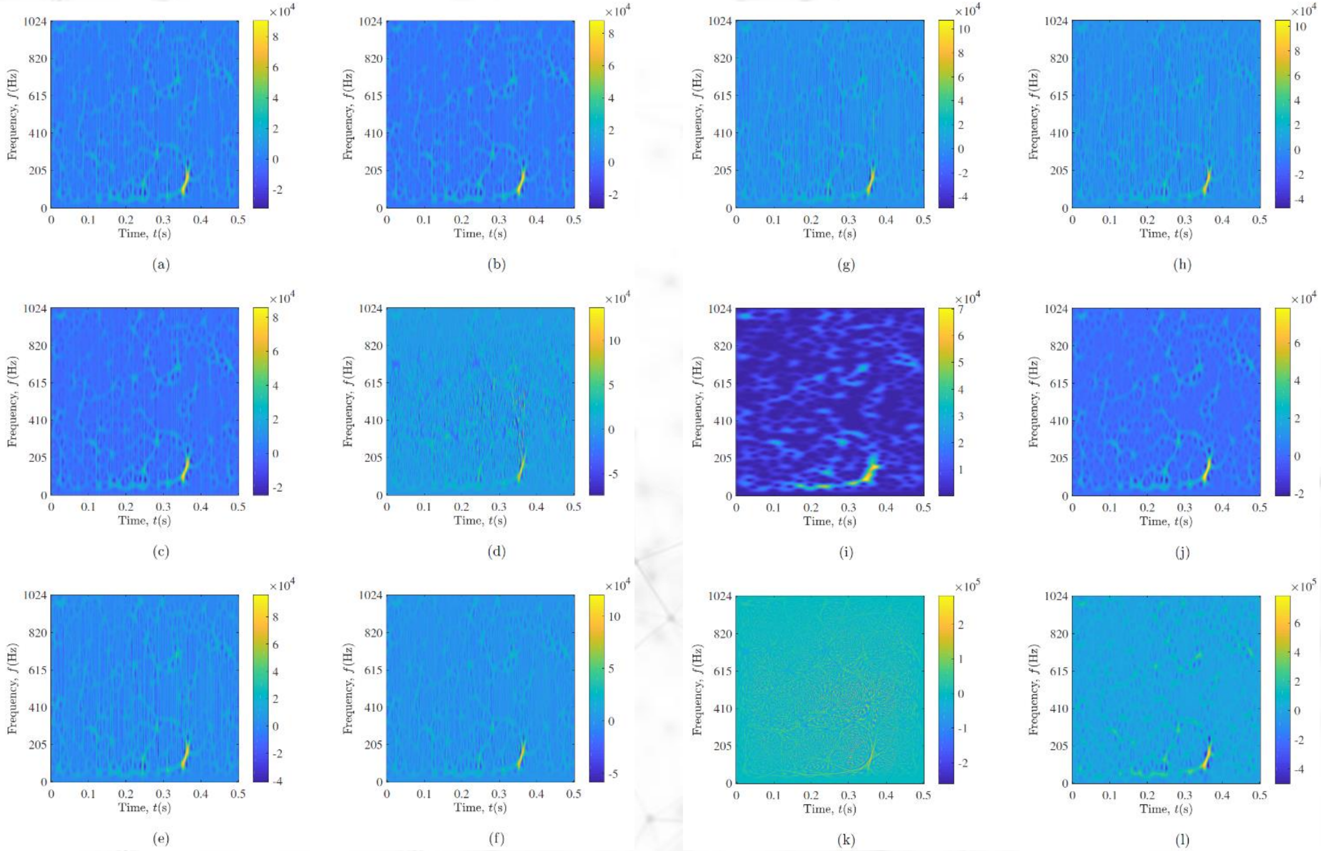

TFDs of the time-series data example containing the GW signal in the noise (NOMF-SNR = 19 dB, OMF-SNR = 14.92 dB): (a) BJD; (b) BUD; (c) CWD; (d) PWVD; (e) RIDB; (f) RIDBN; (g) RIDH; (h) RIDT; (i) SP; (j) SPWVD; (k) WVD; (l) ZAMD.

TFD Calculation

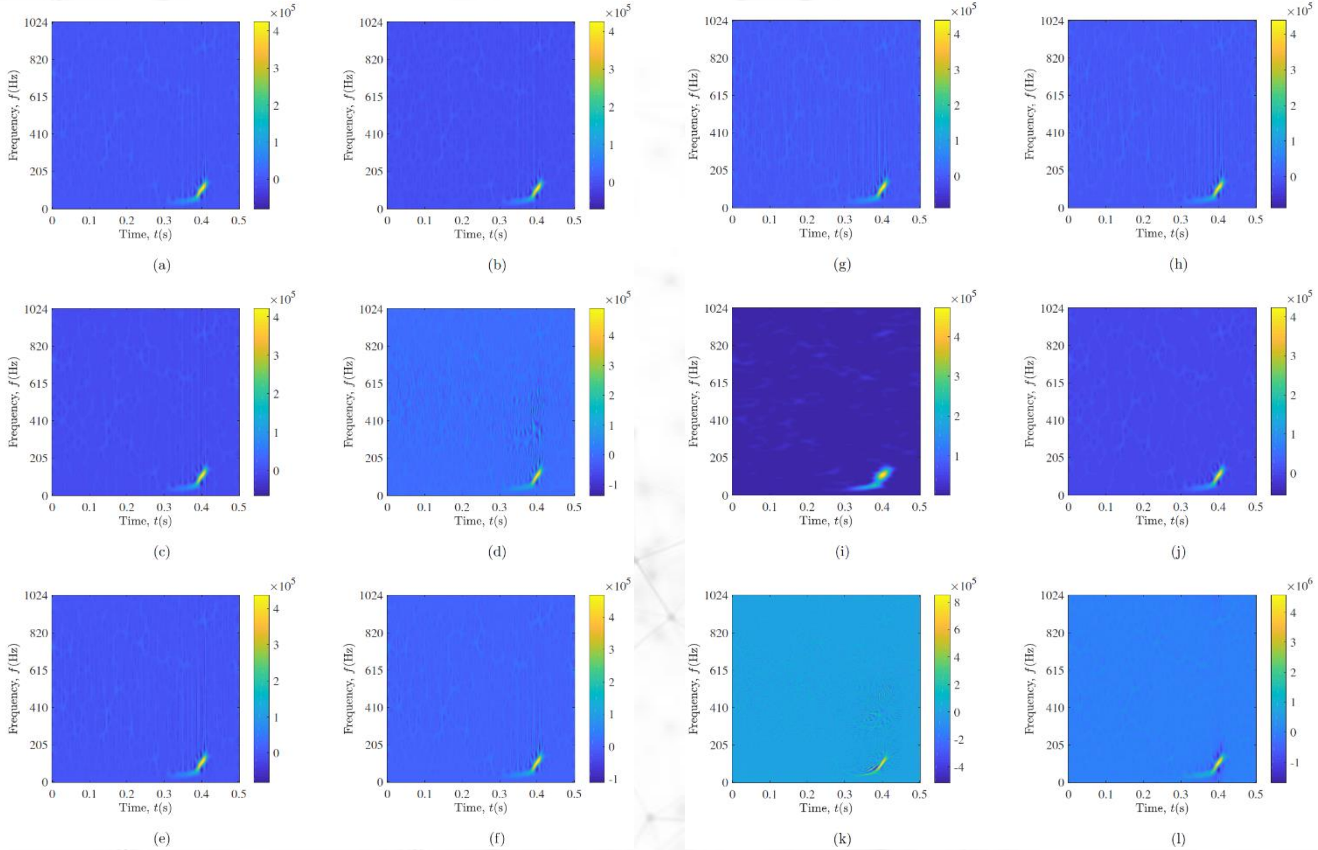

TFDs of the time-series data example containing the GW signal in the noise (NOMF-SNR = 30 dB, OMF-SNR = 25.82 dB): (a) BJD; (b) BUD; (c) CWD; (d) PWVD; (e) RIDB; (f) RIDBN; (g) RIDH; (h) RIDT; (i) SP; (j) SPWVD; (k) WVD; (l) ZAMD.

Deep Learning Classification

Input data

Deep CNN models

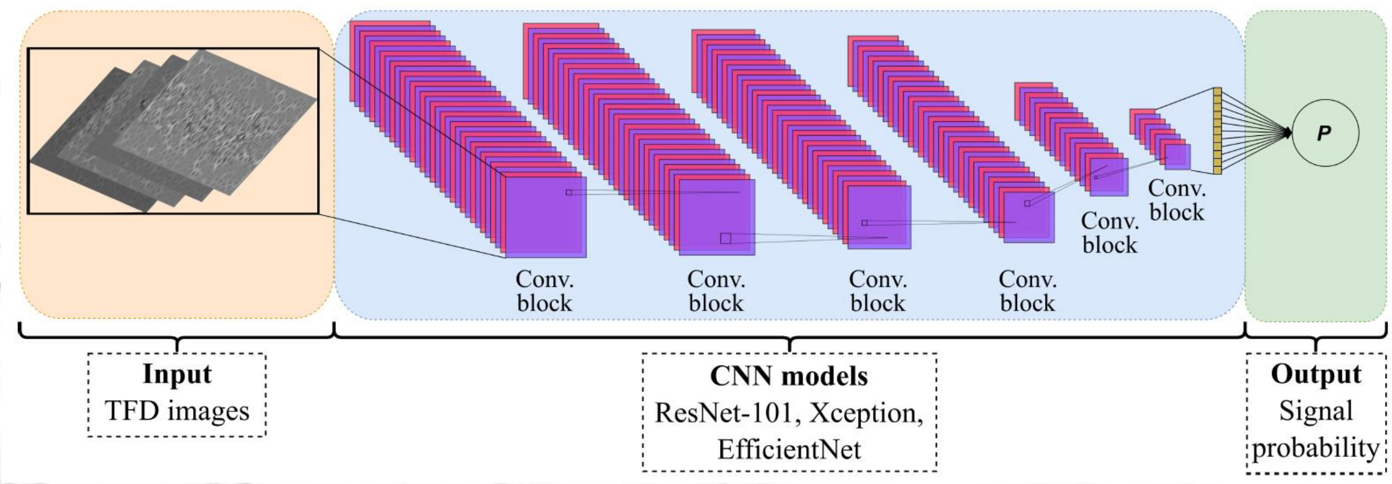

ResNet-101

- Residual (shortcut) connections
- Deep CNN architectures

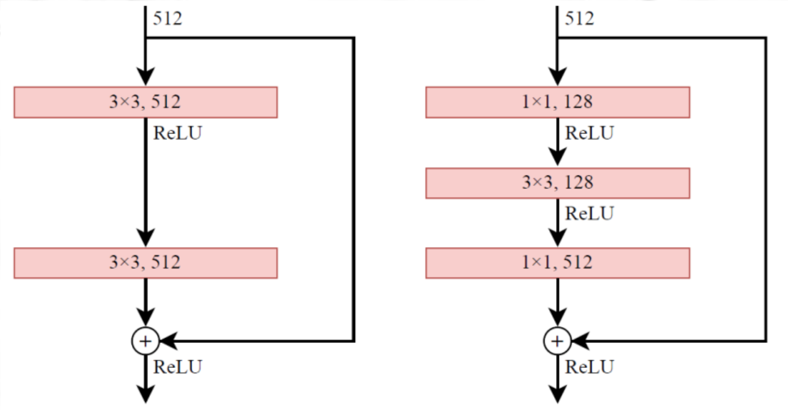

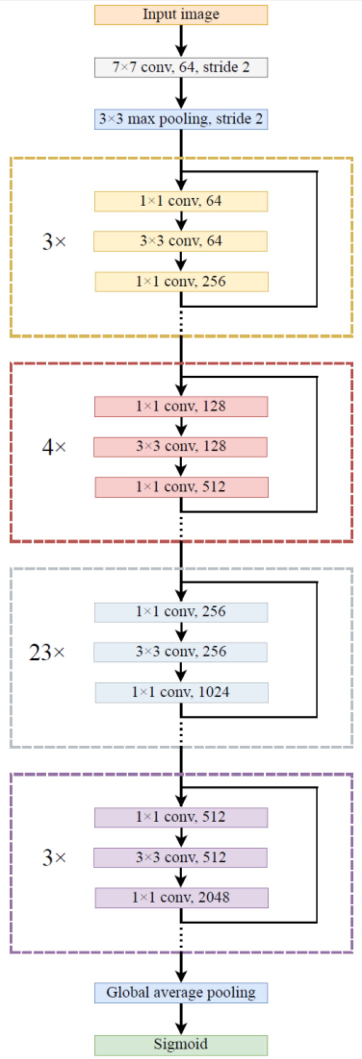

Xception

Depthwise separable convolutions

Residual connections

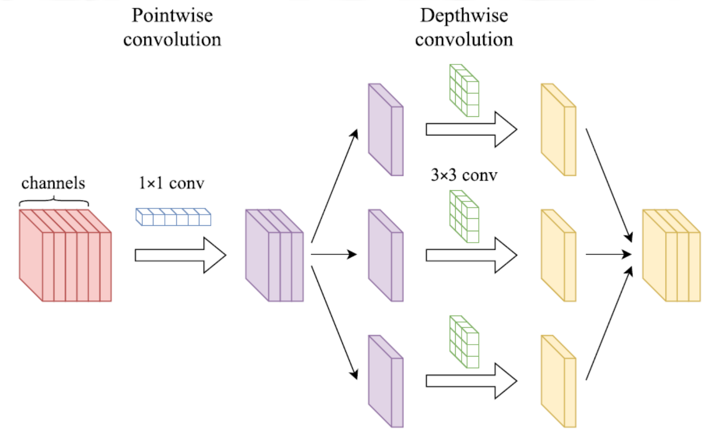

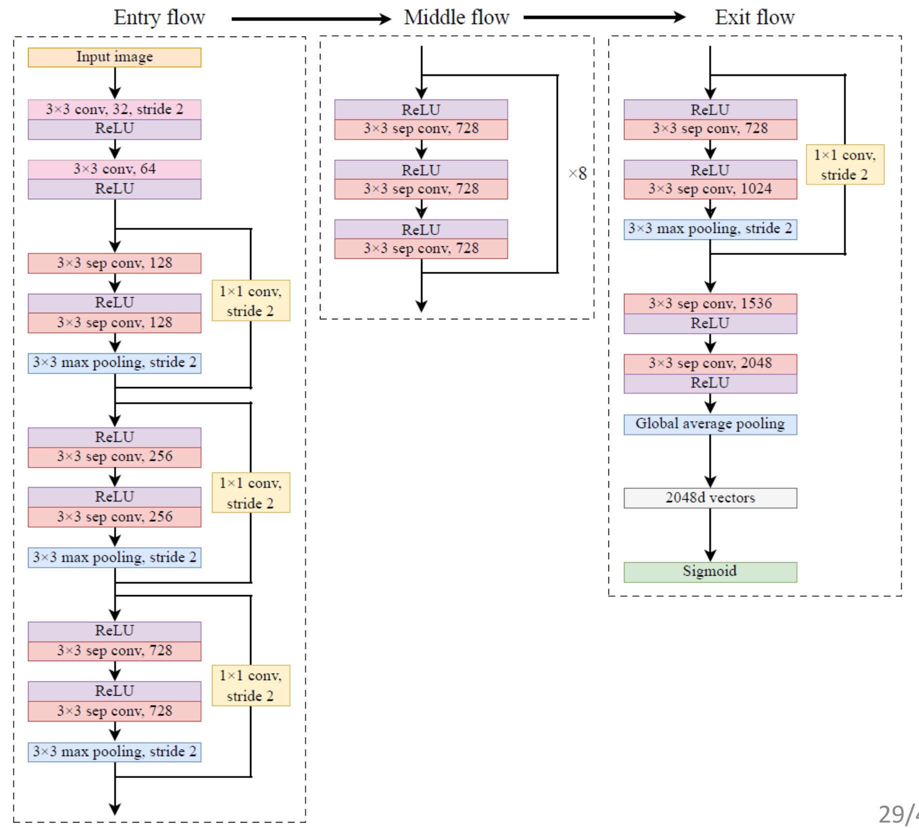

EfficientNet

- Compound scaling
- Mobile inverted bottleneck convolution (MBConv) block
- Squeeze-and-excitation optimization

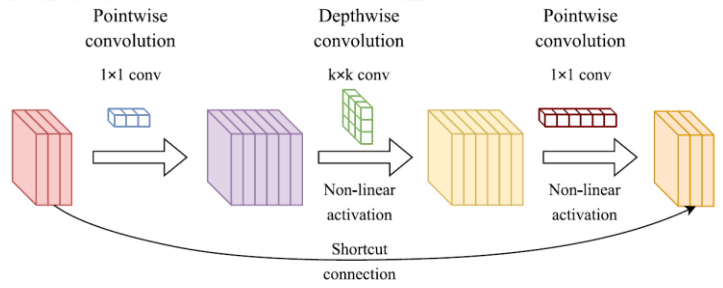

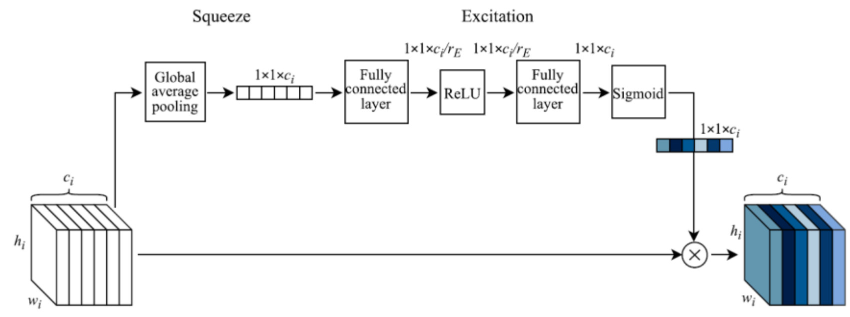

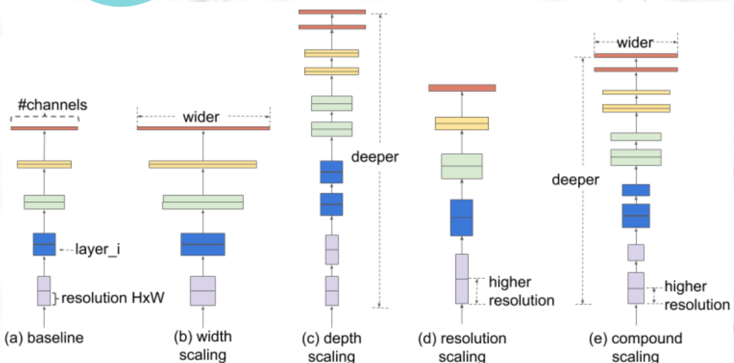

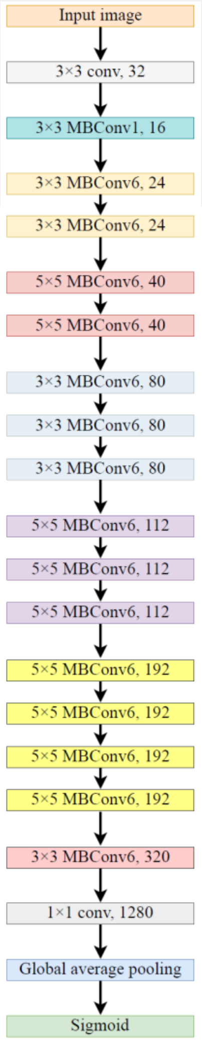

Baseline Model

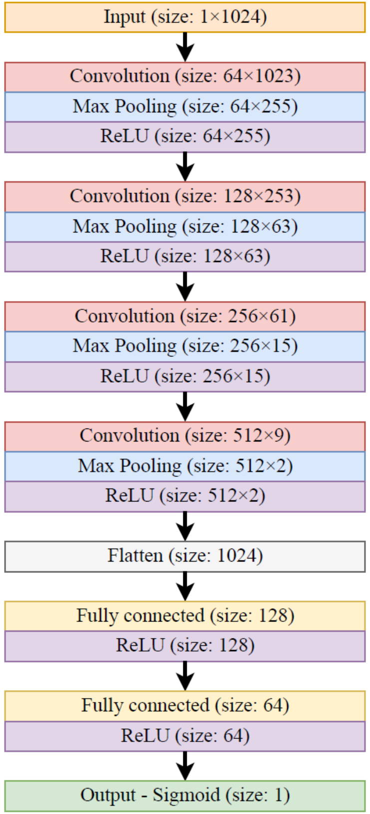

*D. George and E. Huerta, "Deep learning for real-time gravitational wave detection and parameter estimation: Results with Advanced LIGO data," *Physics Letters B*, vol. 778, pp. 64–70, Mar. 2018.

Results

Accuracy & ROC AUC

Accuracy

	CNN architecture		
TFD	**ResNet-101**	**Xception**	**EfficientNet**
BJD	0.96827	0.96800	0.96987
BUD	0.96833	0.96827	0.96893
CWD	**0.96953**	0.96840	0.96980
PWVD	0.96887	0.96967	0.96927
RIDB	0.96853	0.96773	0.96833
RIDBN	0.96927	0.96907	0.96800
RIDH	0.96787	0.96867	0.97000
RIDT	0.96800	0.96860	0.96853
SP	0.96913	0.96953	**0.97100**
SPWVD	0.96760	0.96987	0.96907
WVD	0.96540	**0.97040**	0.96820
ZAMD	0.96813	0.96820	0.96567
Baseline model		0.93147	

- 96.540% (WVD – ResNet-101) → 97.100% (SP – EfficientNet)
- 3.393% → 3.953%

ROC AUC

	CNN architecture		
TFD	**ResNet-101**	**Xception**	**EfficientNet**
BJD	0.98800	0.98708	0.98816
BUD	0.98801	0.98666	0.98686
CWD	0.98703	0.98732	**0.98854**
PWVD	0.98646	0.98729	0.98693
RIDB	**0.98810**	0.98734	0.98637
RIDBN	0.98798	0.98782	0.98754
RIDH	0.98625	0.98753	0.98805
RIDT	0.98711	0.98618	0.98505
SP	0.98727	**0.98810**	0.98823
SPWVD	0.98676	0.98802	0.98766
WVD	0.98539	0.98709	0.98569
ZAMD	0.98708	0.98761	0.98752
Baseline model		0.96787	

- 0.98505 (RIDT – EfficientNet) → 0.98854 (CWD – EfficientNet)
- 1.718% → 2.067%

Recall & Precision

Recall

TFD	CNN architecture ResNet-101	Xception	EfficientNet
BJD	**0.95533**	0.94880	0.94907
BUD	0.95187	0.95147	0.94720
CWD	0.94547	0.94147	0.94787
PWVD	0.94427	0.94947	0.95053
RIDB	0.94493	0.95333	0.94440
RIDBN	0.95067	0.95200	0.94853
RIDH	0.94240	0.94667	0.94947
RIDT	0.94813	0.94973	0.94280
SP	0.94747	0.94453	0.94720
SPWVD	0.95000	0.95120	0.94813
WVD	0.94253	0.95187	0.94467
ZAMD	0.94787	**0.95867**	**0.95533**
Baseline model		0.88853	

- 94.147% (CWD – Xception) → 95.867% (ZAMD – Xception)
- 5.294% → 7.014%

Precision

TFD	CNN architecture ResNet-101	Xception	EfficientNet
BJD	0.98070	0.98669	0.99026
BUD	0.98428	0.98455	0.99024
CWD	**0.99328**	**0.99507**	0.99135
PWVD	0.99313	0.98944	0.98753
RIDB	0.99174	0.98160	0.99188
RIDBN	0.98740	0.98564	0.98696
RIDH	0.99298	0.99024	0.99013
RIDT	0.98736	0.98698	0.99396
SP	0.99038	0.99425	**0.99454**
SPWVD	0.98466	0.98809	0.98956
WVD	0.98770	0.98851	0.99133
ZAMD	0.98791	0.97730	0.97549
Baseline model		0.97200	

- 97.549% (ZAMD – EfficientNet) → 99.507% (CWD – Xception)
- 0.349% → 2.307%

F1 score & PR AUC

F1 score

	CNN architecture		
TFD	**ResNet-101**	**Xception**	**EfficientNet**
BJD	0.96785	0.96737	0.96923
BUD	0.96780	0.96772	0.96824
CWD	**0.96878**	0.96753	0.96912
PWVD	0.96808	0.96904	0.96868
RIDB	0.96777	0.96726	0.96756
RIDBN	0.96868	0.96853	0.96736
RIDH	0.96703	0.96796	0.96937
RIDT	0.96735	0.96800	0.96770
SP	0.96845	0.96875	**0.97029**
SPWVD	0.96702	0.96929	0.96841
WVD	0.96459	**0.96984**	0.96743
ZAMD	0.96747	0.96789	0.96531
Baseline model		0.92839	

- 96.459% (WVD – ResNet-101) → 97.029% (SP – EfficientNet)
- 3.620% → 4.190%

PR AUC

	CNN architecture		
TFD	**ResNet-101**	**Xception**	**EfficientNet**
BJD	0.99159	0.99111	0.99172
BUD	**0.99163**	0.99076	0.99090
CWD	0.99118	0.99125	**0.99195**
PWVD	0.99083	0.99115	0.99090
RIDB	0.99162	0.99119	0.99068
RIDBN	0.99161	0.99148	0.99126
RIDH	0.99059	0.99128	0.99159
RIDT	0.99097	0.99053	0.98989
SP	0.99122	**0.99165**	0.99179
SPWVD	0.99089	0.99161	0.99141
WVD	0.99002	0.99115	0.99012
ZAMD	0.99098	0.99145	0.99127
Baseline model		0.97720	

- 0.98989 (RIDT – EfficientNet) → 0.99195 (CWD – EfficientNet)
- 1.269% → 1.475%

Confusion Matrices

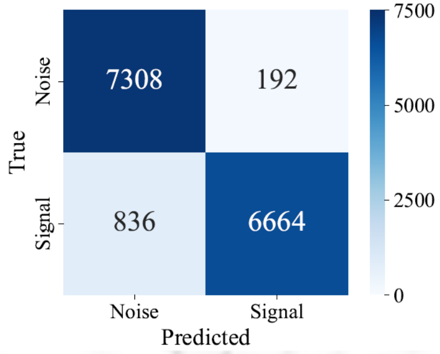

(a)

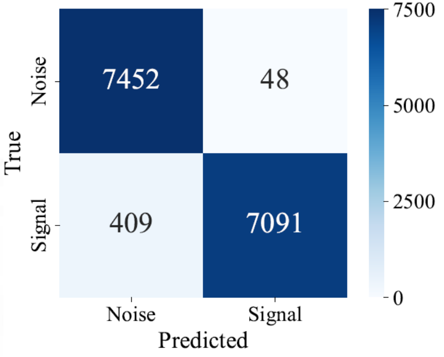

(b)

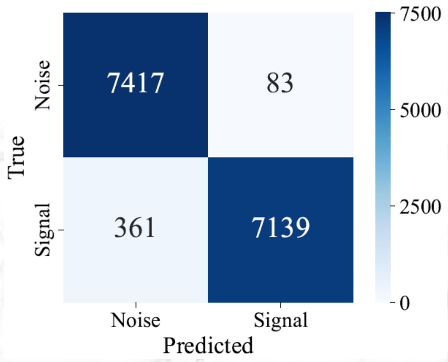

(c)

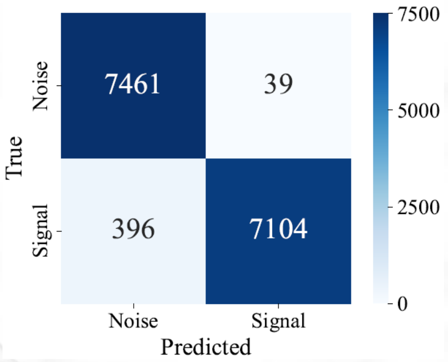

(d)

(a) Baseline model; (b) CWD – ResNet-101; (c) WVD – Xception; (d) SP – EfficientNet.

ROC Curves

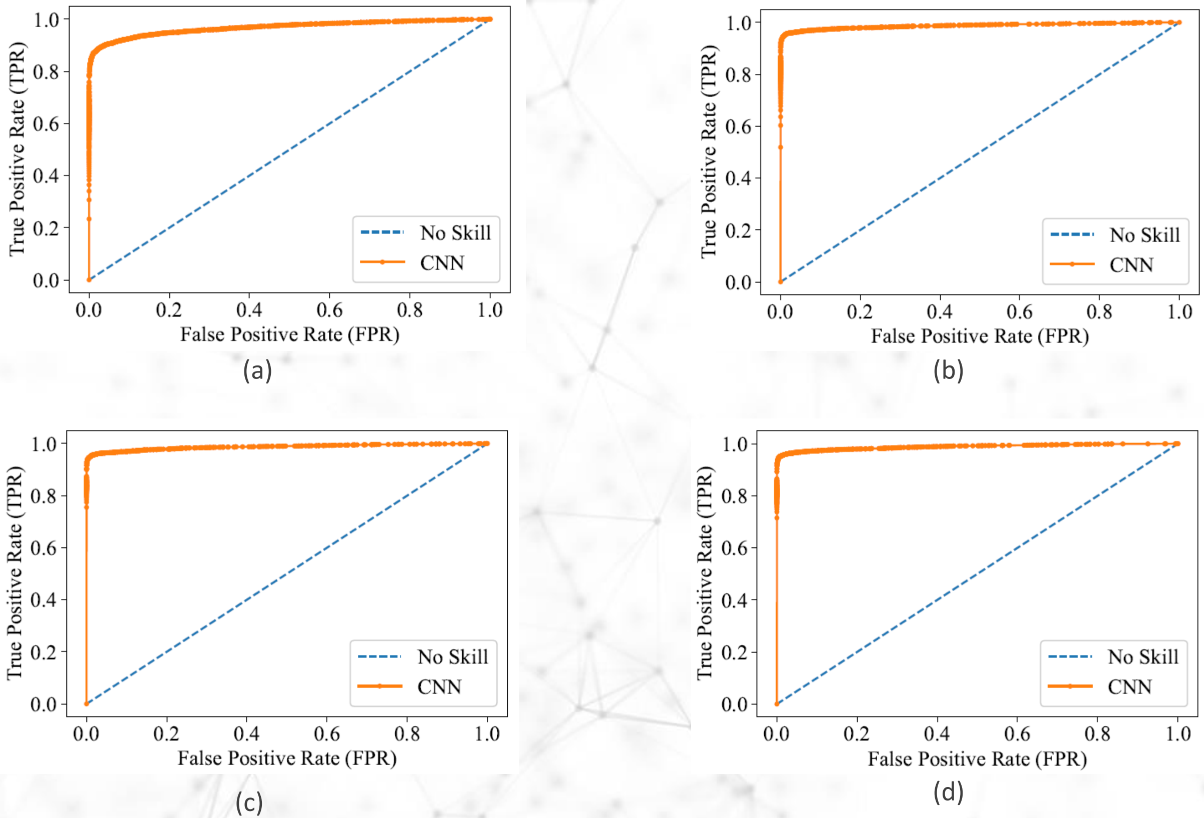

(a) Baseline model; (b) CWD – ResNet-101; (c) WVD – Xception; (d) SP – EfficientNet.

PR Curves

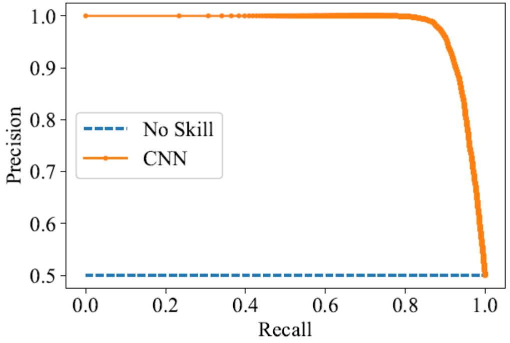

(a)

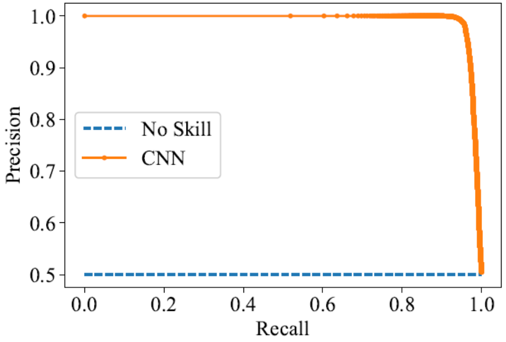

(b)

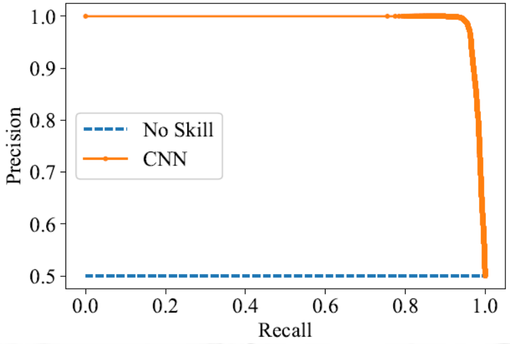

(c)

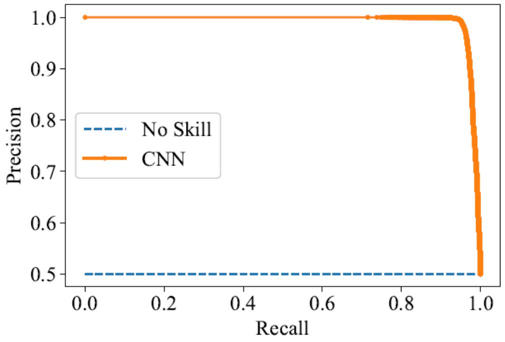

(d)

(a) Baseline model; (b) CWD – ResNet-101; (c) WVD – Xception; (d) SP – EfficientNet.

Conclusions and Future Work

Conclusions and Future Work

Detection of BBH GW signals

Deep CNNs + TFDs from Cohen’s class

Very high classification performances

Better classification performance than the model based on time-series GW signals

Novel modification of Cohen’s class TFD

Data-driven, locally adaptive denoising technique

Publications

N. Lopac, F. Hržić, I. Petrijevčanin Vuksanović, and J. Lerga, “Detection of nonstationary GW signals in high noise from Cohen’s class of time-frequency representations using deep learning,” *IEEE Access*, vol. 10, pp. 2408–2428, Jan. 2022, doi: 10.1109/ACCESS.2021.3139850.

N. Lopac, “Detection of Gravitational-Wave Signals from Time-Frequency Distributions Using Deep Learning,” *Doctoral dissertation*, University of Rijeka, Faculty of Engineering, Mar. 2022.

N. Lopac, J. Lerga, and E. Cuoco, “Gravitational-wave burst signals denoising based on the adaptive modification of the intersection of confidence intervals rule,” *Sensors*, vol. 20, no. 23, Dec. 2020, Art. no. 6920, doi: 10.3390/s20236920.

N. Lopac, J. Lerga, N. Saulig, Lj. Stanković, M. Daković. “On Optimal Parameters for ICI-Based Adaptive Filtering Applied to the GWs in High Noise,” in *2021 6th International Conference on Smart and Sustainable Technologies (SpliTech2021).* Bol and Split, Croatia: IEEE, Sep. 2021, doi: 10.23919/SpliTech52315.2021.9566364.

Bibliography

Bibliography

[1] B. Boashash, Ed., *Time-Frequency Signal Analysis and Processing: A Comprehensive Reference*. London, UK: Academic Press, 2016.

[2] L. Cohen, *Time-Frequency Analysis*. Upper Saddle River, NJ, USA: Prentice Hall PTR, 1995.

[3] L. Stankovic, M. Dakovic, and T. Thayaparan, *Time-Frequency Signal Analysis with Applications*. Boston, MA, USA: Artech House, 2013.

[4] F. Auger, P. Flandrin, P. Gonçalvès, and O. Lemoine, *Time-Frequency Toolbox*. France/USA: CNRS/Rice University, 1996.

[5] N. Lopac, J. Lerga, and E. Cuoco, "Gravitational-wave burst signals denoising based on the adaptive modification of the intersection of confidence intervals rule," *Sensors*, vol. 20, no. 23, Art no. 6920, 2020.

[6] N. Lopac, F. Hržić, I. Petrijevčanin Vuksanović, J. Lerga, "Detection of non-stationary GW signals in high noise from Cohen's class of time-frequency representations using deep learning," *IEEE Access*, vol. 10, pp. 2408–2428, 2022.

[7] Y. LeCun, Y. Bengio, and G. Hinton, "Deep learning," *Nature*, vol. 521, pp. 436–444, 2015.

[8] I. Goodfellow, Y. Bengio, and A. Courville, *Deep Learning*. Cambridge, MA, USA: MIT Press, 2016.

[9] K. He, X. Zhang, S. Ren, and J. Sun, "Deep residual learning for image recognition," in *2016 IEEE Conference on Computer Vision and Pattern Recognition (CVPR 2016)*, Las Vegas, NV, USA: IEEE, 2016, pp. 770–778.

[10] F. Chollet, "Xception: Deep learning with depthwise separable convolutions," in *2017 IEEE Conference on Computer Vision and Pattern Recognition (CVPR 2017)*. Honolulu, HI, USA: IEEE, 2017, pp. 1800–1807.

[11] M. Tan and Q. Le, "EfficientNet: Rethinking model scaling for convolutional neural networks," in *36th International Conference on Machine Learning (ICML 2019).* Long Beach, CA, USA: PMLR, 2019, pp. 6105–6114.

[12] M. Sandler, A. Howard, M. Zhu, A. Zhmoginov, and L.-C. Chen, "MobileNetV2: Inverted residuals and linear bottlenecks," in *2018 IEEE/CVF Conference on Computer Vision and Pattern Recognition (CVPR 2018)*. Salt Lake City, UT, USA: IEEE, 2018, pp. 4510–4520.

Bibliography

[13] J. Hu, L. Shen, and G. Sun, “Squeeze-and-excitation networks,” in *2018 IEEE/CVF Conference on Computer Vision and Pattern Recognition (CVPR 2018)*. Salt Lake City, UT, USA: IEEE, 2018, pp. 7132–7141.

[14] LIGO Caltech. LIGO: Laser Interferometer Gravitational-Wave Observatory, (accessed Sep. 29, 2021). [Online]. Available: https://www.ligo.caltech.edu/.

[15] J. Aasi *et al.*, “Advanced LIGO,” *Classical and Quantum Gravity*, vol. 32, no. 7, Art. no. 074001, 2015.

[16] S. A. Usman *et al.*, “The PyCBC search for gravitational waves from compact binary coalescence,” *Classical and Quantum Gravity*, vol. 33, no. 21, Art no. 215004, 2016.

[17] E. Cuoco *et al.*, “Enhancing gravitational-wave science with machine learning,” *Machine Learning: Science and Technology*, vol. 2, no. 1, Art no. 011002, 2020.

[18] D. George and E. A. Huerta, “Deep neural networks to enable real-time multimessenger astrophysics,” *Physical Review D*, vol. 97, no. 4, Art no. 044039, 2018.

[19] D. George and E. A. Huerta, “Deep Learning for real-time gravitational wave detection and parameter estimation: Results with Advanced LIGO data,” *Physics Letters B*, vol. 778, pp. 64–70, 2018.

[20] H. Gabbard, M. Williams, F. Hayes, and C. Messenger, “Matching matched filtering with deep networks for gravitational-wave astronomy,” *Physical Review Letters*, vol. 120, no. 14, 2018, Art. no. 141103.

[21] T. D. Gebhard, N. Kilbertus, I. Harry, and B. Schölkopf, “Convolutional neural networks: A magic bullet for gravitational-wave detection?” *Physical Review D*, vol. 100, no. 6, 2019, Art. no. 063015.

[22] LIGO Scientific Collaboration, “LIGO Algorithm Library - LALSuite,” 2018.

[23] LIGO Scientific Collaboration, “The O2 Data Release,” 2019.

Thank you for your attention!

Questions?